frontiers in Physics

ORIGINAL RESEARCH
published: 20 November 2018
doi: 10.3389/fphy.2018.00131

Intracellular Mass Density Increase Is Accompanying but Not Sufficient for Stiffening and Growth Arrest of Yeast Cells

*Shada Abuhattum[1,2†], Kyoohyun Kim[1†], Titus M. Franzmann[3], Anne Eßlinger[3], Daniel Midtvedt[4], Raimund Schlüßler[1], Stephanie Möllmert[1], Hui-Shun Kuan[5,6], Simon Alberti[3], Vasily Zaburdaev[5,6] and Jochen Guck[1]**

[1] Biotechnology Center, Center for Molecular and Cellular Bioengineering, Technische Universität Dresden, Dresden, Germany, [2] JPK Instruments AG, Berlin, Germany, [3] Max Planck Institute of Molecular Cell Biology and Genetics, Dresden, Germany, [4] Department of Applied Physics, Chalmers University of Technology, Gothenburg, Sweden, [5] Max Planck Institute for the Physics of Complex Systems, Dresden, Germany, [6] Department of Biology, Friedrich-Alexander Universität Erlangen-Nürnberg, Erlangen, Germany

OPEN ACCESS

Edited by:
Giancarlo Ruocco,
Istituto Italiano di Tecnologia (IIT),
Center for Life NanoScience, Italy

Reviewed by:
Giovanni Cappello,
Centre National de la Recherche Scientifique (CNRS), France
Barbara Cortese,
Istituto di Nanotecnologia (NANOTEC), Italy

***Correspondence:**
Jochen Guck
jochen.guck@tu-dresden.de

[†] These authors have contributed equally to this work

Specialty section:
This article was submitted to Condensed Matter Physics, a section of the journal Frontiers in Physics

Received: 01 August 2018
Accepted: 30 October 2018
Published: 20 November 2018

Citation:
Abuhattum S, Kim K, Franzmann TM, Eßlinger A, Midtvedt D, Schlüßler R, Möllmert S, Kuan H-S, Alberti S, Zaburdaev V and Guck J (2018) Intracellular Mass Density Increase Is Accompanying but Not Sufficient for Stiffening and Growth Arrest of Yeast Cells. Front. Phys. 6:131. doi: 10.3389/fphy.2018.00131

Many organisms, including yeast cells, bacteria, nematodes, and tardigrades, endure harsh environmental conditions, such as nutrient scarcity, or lack of water and energy for a remarkably long time. The rescue programs that these organisms launch upon encountering these adverse conditions include reprogramming their metabolism in order to enter a quiescent or dormant state in a controlled fashion. Reprogramming coincides with changes in the macromolecular architecture and changes in the physical and mechanical properties of the cells. However, the cellular mechanisms underlying the physical–mechanical changes remain enigmatic. Here, we induce metabolic arrest of yeast cells by lowering their intracellular pH. We then determine the differences in the intracellular mass density and stiffness of active and metabolically arrested cells using optical diffraction tomography (ODT) and atomic force microscopy (AFM). We show that an increased intracellular mass density is associated with an increase in stiffness when the growth of yeast is arrested. However, increasing the intracellular mass density alone is not sufficient for maintenance of the growth-arrested state in yeast cells. Our data suggest that the cytoplasm of metabolically arrested yeast displays characteristics of a solid. Our findings constitute a bridge between the mechanical behavior of the cytoplasm and the physical and chemical mechanisms of metabolically arrested cells with the ultimate aim of understanding dormant organisms.

Keywords: yeast, optical diffraction tomography, atomic force microscopy, refractive index, stiffness, liquid solid transition

INTRODUCTION

Eukaryotic cells form compartments and organelles to spatially and temporally organize their cellular contents [1, 2]. Many of these compartments such as nuclei, lysosomes, mitochondria, and endoplasmic reticulum are bound by a lipid bilayer. Yet, recent studies have suggested that several types of organelles are not delimited by a lipid bilayer, but formed by liquid–liquid

phase separation, where the dense phase of macromolecules such as RNAs and proteins are concentrated spontaneously from the surrounding solution [3, 4]. A growing number of organelles have been reported as such membrane-less compartments, including nucleolus for ribosome biogenesis and stress response, and P bodies for RNA storage and degradation [2]. The liquid–liquid phase separation process can be tightly regulated by the cell owing its sensitive dependence on internal material concentration. However, under certain circumstances, these membrane-less compartments can also undergo liquid-to-solid phase transitions to form aberrant solid aggregates. For instance, when the genes encoding for the constituting macromolecules carry specific mutations, this phase transition is associated with neurodegenerative diseases via amyloid-like assembly of RNA binding protein Fused in Sarcoma (FUS) [5].

Liquid-to-solid phase transitions are not always pathological. Some organisms change their physical properties from a liquid- to solid-like state when faced with unfavorable conditions to facilitate survival. In this state, typically referred to as dormancy, the cell cycle is arrested and metabolic activity is reduced or suspended, but the cell can still recover to normal physiology and function when the conditions are favorable again. For example, plants develop seeds that survive cold and dry weather and germinate in spring [6]. Bacteria form metabolically inactive spores that are highly resistant to stress and antibiotics [7]. *Caenorhabditis elegans* enter a dauer stage that relies entirely on internal energy sources for as long as 4 months [8]. And finally, yeast cells compact their cytoplasm and cease proliferation in the absence of energy [9, 10]. These changes in the function of the organism are associated with drastic alterations of the cellular architecture.

Yeast cells undergo metabolic and morphological changes when faced with various types of stresses including temperature changes, osmotic, and oxidative pressure [11, 12]. Delaraue et al. demonstrated that external compression exerted on yeast cells as a result of self-driven confinement leads to slow down in cell growth and delay of cell cycle progression in the G1 phase [13]. Also, Munder et al. showed recently that lowering the intracellular pH of yeast cells, which is a consequence of lack of energy, promotes entry into dormancy [14]. When the cytosol was in acidic pH, the cells reduced their volume and formed macromolecular assemblies. These cells exhibited a reduction in the mobility of organelles and exogenous tracer particles, and were measurably stiffer than active cells. Yet, it is still unclear how they acquire this increased mechanical stability associated with dormancy. Is an increase in the intracellular mass density sufficient for a liquid-to-solid transition, which could then be associated with a glass-transition above a critical volume fraction? Or does it involve the assembly of macromolecules to form a percolated, solid-like intracellular matrix? In this study, we adopt the same technique of Munder et al. to arrest growth in fission yeast cells by lowering intracellular pH. We evaluate the physical properties of yeast cells optical diffraction tomography (ODT) and atomic force microscope (AFM) for probing their mass density and mechanical properties, respectively. We show that metabolically arrested cells exhibit higher intracellular mass density as well as elevated cell stiffness. However, an increased intracellular mass density alone is not sufficient to maintain cells in growth arrest. Thus, we suggest that yeast, when challenged by extreme conditions, utilizes distinct supramolecular structures in its dense cytoplasm that induce an increased mechanical stability.

MATERIALS AND METHODS

Yeast Cell Culture and Growth Assay

Schizosaccharomyces pombe strain ED668 was grown and maintained on YES (Formedium) agar plates at low temperatures. Two days prior to measurement, 50 mL liquid YES and 50 mL YES supplemented with 1.2 M sorbitol (Sigma) were inoculated with single colonies and incubated shaking at 180 rpm at 30°C overnight, respectively. The overnight cultures were then used to inoculate both, 50 mL YES and 50 mL YES supplemented with 1.2 M sorbitol at an optical density of $OD_{600\,nm} = 0.05$, respectively, and grown to early mid-log phase $OD_{600\,nm} = 0.2$–0.4. The later was intended for adapting the cells to a hypertonic growth medium. Note that YES is a rich medium that contains glucose. For particle tracking analysis, *S. cerevisiae* cells grown at 25 or 30°C in yeast extract peptone dextrose (YPD) were used.

pH Adjustment of Cells

The pH adjustment of the yeast cytosol was carried out as described previously [10, 14]. Briefly, a set of either 100 mM potassium phosphate, 2% glucose, or 40 mM PIPES, 2% glucose was prepared at different pH-values. Yeast cells from a liquid culture were centrifuged for 10 s at 2,000 rcf and washed once with the buffer to remove residuals of culture medium. The cells were then resuspended in the respective buffer supplemented with 2 mM 2,4-dinitrophenol (DNP) in order to equilibrate the intracellular pH with the extracellular pH. Omitting DNP from the sample served as controls. The pH values used range between 6.0 and 7.6.

Spheroplasting (Cell Wall Removal)

Early mid-log cells were harvested by centrifugation (4 min at 1,500 rcf) and resuspended in 100 mM phosphate buffer supplemented with 1.2 M sorbitol and 2% glucose. To remove the cell wall, 0.5 mg/mL Zymolyase 100T (ZymoLabs) and 2.5 mg/mL lysing enzymes from *Trichoderma harzianum* (Sigma) were added to the PBS medium and the reaction was incubated for ∼120 min. Spheroplasts were then resuspended in 100 mM potassium phosphate buffer pH 6.0 or pH 7.5, respectively. Two millimolar of DNP were added as described in the previous section. Spheroplasting removes the very stiff cell wall (but not the cell membrane) of yeast cells so that the cell stiffness can be determined by indentation tests. Sorbitol is required in the medium after spheroplasting to prevent the cells from bursting.

Optical Diffraction Tomography (ODT)

The three-dimensional (3D) refractive index (RI) distribution of samples was measured using a custom-made ODT microscope. The optical setup of ODT employs Mach-Zehnder interferometry in order to measure complex optical fields of light scattered by samples from various incident angles, as shown in (**Figure 1A**).

A coherent laser beam ($\lambda = 532$ nm, frequency-doubled Nd-YAG laser, Torus, Laser Quantum, Inc., UK) is divided into two beams by a 2×2 single-mode fiber optic coupler. One beam is used as a reference beam and the other beam illuminates the specimen on the stage of a custom-made inverted microscope through a tube lens ($f = 175$ mm) and a high numerical aperture (NA) objective lens (NA = 1.2, 63×, water immersion, Carl Zeiss AG, Germany). To reconstruct a 3D RI tomogram of samples in a field-of-view, the samples are illuminated with 150 various incident angles scanned by a dual-axis galvanomirror (GVS012/M, Thorlabs Inc., USA). The diffracted beam from a sample is collected by a high NA objective lens (NA = 1.3, 100×, oil immersion, Carl Zeiss AG) and a tube lens ($f = 200$ mm). The total magnification is set to be 90.5×. The beam diffracted by the sample interferes with the reference beam at an image plane, and generates a spatially modulated hologram. The hologram is recorded with a CCD camera (FL3-U3-13Y3M-C, FLIR Systems, Inc., USA).

The complex optical fields of light scattered by the samples were retrieved from the recorded holograms by applying a Fourier transform-based field retrieval algorithm as previously published [15, 16]. The 3D RI distribution of the samples was reconstructed from the retrieved complex optical fields via the Fourier diffraction theorem. A more detailed description of tomogram reconstruction can be found elsewhere [17–20]. From the reconstructed RI tomograms, the individual yeast cells were segmented by applying Otsu's method and a watershed segmentation algorithm, and the mean RI-value inside the binary image of an individual yeast cell was determined. The mass density of individual yeast cells is directly calculated from the mean RI-value, since the RI-value in biological samples is linearly proportional to the mass density inside cells as $n(x,y,z) = n_m + \alpha C(x,y,z)$, where $n(x,y,z)$ is the 3D RI distribution of samples, n_m is the RI-value of the surrounding medium ($n_m = 1.339$ at $\lambda = 532$ nm), α is an RI increment ($\alpha = 0.190$ mL/g for protein [21]), and $C(x,y,z)$ is the mass density inside cells. All tomogram acquisition and data analysis were performed using a custom-written MATLAB code.

Atomic Force Microscopy (AFM) Measurements

AFM-based nanoindentation measurements were performed using a Nanowizard 4 (JPK Instruments) and an optical inverted microscope (Observer D1, Zeiss). For immobilizing the spheroplasts of *S. pombe* prior to the measurement, CellTak (Corning), a cell adhesive protein solution, was first applied to the plastic petri dish and then rinsed for removing residuals [22]. Measurements were carried out using a wedged cantilever that is parallel to the petri dish as illustrated in **Figure 1B**. This simplifies indenting spherical cells, prevents their movement during the procedure and compensates for the original 10° angle of the glass blocks used for mounting the cantilevers. The wedged cantilever was prepared using a UV curing glue that was applied to tipless cantilevers (PNP-TR-TL, nominal spring constant $k = 0.32$ N/m, Nanoworld, or HQ: CSC37/tipless/No Al, nominal spring constant $k = 0.3$ N/m, Mikromasch). For determining cell stiffness, the cantilever was positioned above a single spheroplast and lowered with a speed of 5 μm/s. Force-distance curves were recorded until an indentation of 0.3–0.8 μm was reached (1.5–4 nN). All measurements were carried out in the 100 mM phosphate buffer containing 1.2 M sorbitol, 2% glucose, and DNP at 30°C.

AFM-based Indentation Data Analysis

The force-distance curves were analyzed using JPK data processing software. First, the curves' baseline was adjusted and the data were corrected for the tip-sample separation [23]. Then each curve was fitted with the Hertz model modified by Sneddon for a spherical geometry to evaluate the spherical spheroplasts as shown in **Figure 1C** [24, 25] using

$$F = \frac{E}{1-\nu^2} \times \left(\frac{R^2 + r^2}{2} \ln \frac{r+R}{r-R} - Rr \right) \text{ and} \quad (1)$$

$$\delta = \frac{R}{2} \ln \left(\frac{r+R}{r-R} \right), \quad (2)$$

where F denotes the indentation force, δ the indentation depth, r the cell radius, $R = \sqrt{\delta r}$ the radius of the circular contact area, and ν is the Possion's ratio and is set to 0.5 in all measurements.

The radius of the cells was measured for each of the cell groups and the average radius was used for each individual group (ranging between $r = 2.28$–2.45 μm) shown in the inset in **Figure 1C**. The apparent Young's modulus extracted from the fit was corrected for the additional stress that the cells encounter from the bottom of the plate, which causes an additional deformation of the spherical shape [26, 27]. The Young's modulus is reported as "apparent," acknowledging the fact that some of the Hertz model assumptions are not met such as isotropic and homogeneous samples. While the absolute values are debatable, this approach still serves well the aim of quantitative comparison.

Osmolality

Osmolality measurements of mediums and buffers used were carried out using an Osmomat 3000 Freezing point osmometer (Gonotec). Three independent measurements were carried out per sample and averaged to calculate the mean and standard deviation.

Particle Tracking

For particle tracking in budding yeast (*S. cerevisiae*), we made use of a genetically encoded viral capsid protein (GFP − μ NS) which self-assembles into distinct particles in the yeast cytoplasm [14]. These particles were subsequently imaged on an Andor Spinning disk setup [Olympus IX71 stand, Olympus UPlanSApo 60x oil objective, resulting pixel size $(x, y) = 108$ nm]. Particle tracking was performed using the open source Fiji plugin MosaicSuite particle tracker [28]. Analysis of the tracked particles was performed in MATLAB.

Statistical Analysis

To perform statistical analysis on ODT and AFM experiments we measured three independent sets of yeast cells. The mean values were subjected to statistical analysis by the two-tailed Mann-Whitney U-test using python Scipy library. The shown asterisks indicate significance levels: $^{*}p < 0.01$, $^{**}p < 0.001$, $^{***}p < 0.0001$.

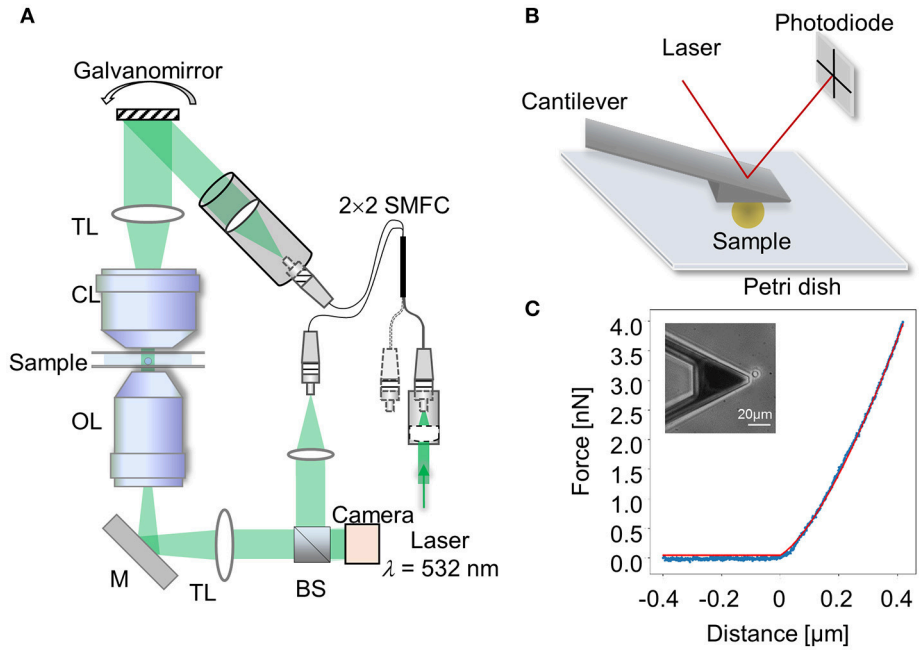

FIGURE 1 | Experimental setups. **(A)** Schematic diagram of the optical setup for optical diffraction tomography (ODT). SMFC, single-mode fiber coupler; TL, tube lens; CL, condenser lens; OL, objective lens; M, mirror; BS, beam splitter. **(B)** Schematic diagram of atomic force microscopy (AFM) using a wedged cantilever to indent a spherical sample. **(C)** Representative force-distance curve (blue dotted line) recorded during compression with a wedged cantilever shown in inset. Hertz model fit (red solid line) to extract the apparent Young's Modulus.

RESULTS

Yeast cells usually grow in acidic environments and use proton-translocating ATPases for maintaining their intracellular pH neutral at the expense of large amounts of energy in the form of ATP hydrolysis. When energy is scarce, however, these cells enter into a dormant state [29–32]. In dormancy, the cytosol becomes acidic as the supply of ATP is not sufficient to maintain the proton pumping [9, 10, 14]. We have shown that lowering the intracellular pH, by incubating the cells in acidic buffers and adding protonophores, such as DNP, that carry protons across the membrane, promotes entry into a dormant state in both fission and budding yeast cells, even if energy is present [14]. As a consequence of reducing intracellular pH, two main changes occur in the cell cytoplasm. First, a large fraction of cytosolic proteins reduces the net charge, becomes less soluble and forms aggregates, and second, the cell displays a reduction in volume and an increase in cytoplasmic crowding. Both processes can potentially lead to an increase in the mechanical stability of the cytoplasm in the liquid-to-solid transition that is observed, either mediated by the formation of a percolated cellular matrix of supramolecular assemblies (similar to a sol-gel transition) or by the increase in mass density after volume loss above a critical value, leading to a glass-like state. Here, we focus on fission yeast and decouple these two scenarios by designing a set of experiments to independently change intracellular pH and volume of yeast cells. We start by examining the effects of either pH changes or osmotic pressure on mass density using ODT. We then combine both effects to understand their mutual contribution to growth arrest of cells. Finally, we compare the mass density to the stiffness measurements done using AFM to determine whether an increased mass density is sufficient to drive cells into the mechanically stable state associated with dormancy.

Lowering Intracellular pH Increases Mass Density of Yeast Cells

We have previously shown that lowering the intracellular pH promotes entry into dormancy and is coupled with volume decrease [14]. However, it is still unclear whether cells with low intracellular pH simply expel water and increase overall intracellular mass density or whether they also decrease the non-aqueous cytoplasmic content. Here, we investigated the effect of this pH reduction on intracellular mass density. We used ODT to measure the RI-values from which we calculated directly the mass density (see Methods and Materials section) of yeast cells in media with different pH-values starting from neutral pH 7.6 to acidification of the cytoplasm at pH 6.0 (see **Figure 2A**). The pH of the cytoplasm was adjusted by resuspending the cells in a buffer with the respective pH that contained DNP in order to equilibrate the intracellular pH with the extracellular pH (see Materials and methods Section pH adjustment of cells). As a control, we incubated the cells at two pH values (pH 6.0 and pH 7.6) in the absence of DNP so that the intracellular pH in the cells remained neutral. **Figure 2B** shows that the mean RI-values of yeast were increased in the pH range of 6.2–6.4 compared to the other, more

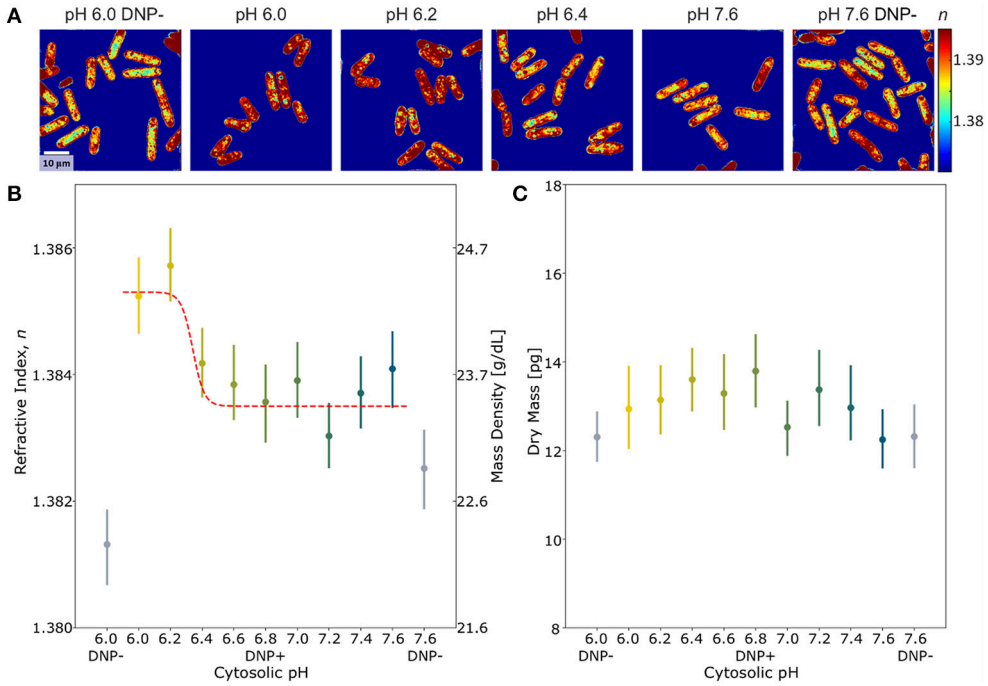

FIGURE 2 | The effect of intracellular pH on the refractive index and dry mass of *S. pombe*. **(A)** Typical cross-sectional slices of the 3D refractive index tomograms of yeast cells in the *x-y* plane. Two control groups of cells incubated at pH 6.0 and 7.6 in the absence of DNP are denoted by DNP^{-}. The scale bar indicates 10 µm. **(B–C)** The mean refractive index (RI) distribution **(B)** and the dry mass content **(C)** of yeast cells at different intracellular pH. the points shown correspond to the mean refractive index or dry mass measured at that pH value and lines indicate error bars (for each pH condition, $N > 95$).

neutral pH-values. The sigmoidal fit illustrates the cooperativity of this behavior. In contrast, the dry mass stayed constant for all values of intracellular pH (see **Figure 2C**), which suggests that lowering intracellular pH increases the intracellular mass density as a result of volume decrease (see **Supplementary Figure 1**).

To understand the biochemistry of the cytosolic proteins of *S. pombe* in different intracellular pH-values, we calculated the distribution of the isoelectric points of all proteins in the *S. pombe* yeast proteome, as was done in our previous study by Munder et al. [14]. We found that the isoelectric points of yeast proteins are clustered in two peaks one in the acidic range and the other in the basic range, excluding the neutral pH (see **Supplementary Figure 2**). This may suggest that many proteins reduce their net charge in low pH, become less soluble and form aggregates in the cytoplasm. However, it still remains unknown whether a reduction in volume and the associated increase in intracellular mass density alone would lead to stiffness changes associated with cells entering dormancy.

Cytoplasmic Crowding Is Insufficient For Promoting Growth Arrest

Next, we applied osmotic pressure on yeast cells without changing their intracellular pH to examine whether high intracellular mass density triggers dormancy. We measured RI tomograms of yeast cells grown in YES medium as a control (osmolality 0.196 ± 0.001 Osmol/kg, see **Figure 3A**), and compared their RI tomograms with those obtained for cells after adding 1.2 M sorbitol to YES medium (osmolality 1.946 ± 0.008 Osmol/kg which corresponds to an osmotic pressure of ∼ 3.9MPa, see **Figure 3B**) as well as with those for cells that had adapted to osmotic pressure overnight (**Figure 3C**).

Figure 3D shows that the mean RI value of yeast cells increases immediately upon osmotic stress, from 1.3840 ± 0.0002 (mean ± SEM) to 1.4190 ± 0.0004, however, it recovers to 1.3950 ± 0.0003 as the cells adapt to osmotic pressure overnight. The RI changes are associated with the change of cell volume, as the yeast cells shrink upon osmotic stress from 66 ± 2 to 44 ± 2 fL and recover to a volume of 60 ± 2 fL after the adaptation to osmotic pressure (**Figure 3E**). Moreover, the dry mass of yeast cells increases upon osmotic stress from 15.0 ± 0.4 to 18.2 ± 0.7 pg and then maintains a similar dry mass of 17.7 ± 0.6 pg during the osmotic adaptation (**Figure 3F**). The initial increase of the dry mass after osmotic shock can be attributed to two processes. In short times the sorbitol molecule might diffuse into the cytoplasm, consecutively cells produce additional substances such as trehalose or glycerol as a protection mechanism from osmotic stress [33, 34]. The addition of material leads to a slight increase of the mean RI-value of osmotically adapted yeast cells compared to controls grown in YES medium. Here, we show that cells adapt to and grow in a hypertonic medium despite high-density values even exceeding those exhibited by lowering intracellular pH. This finding implies that increasing intracellular mass density to values similar to, or even beyond those associated

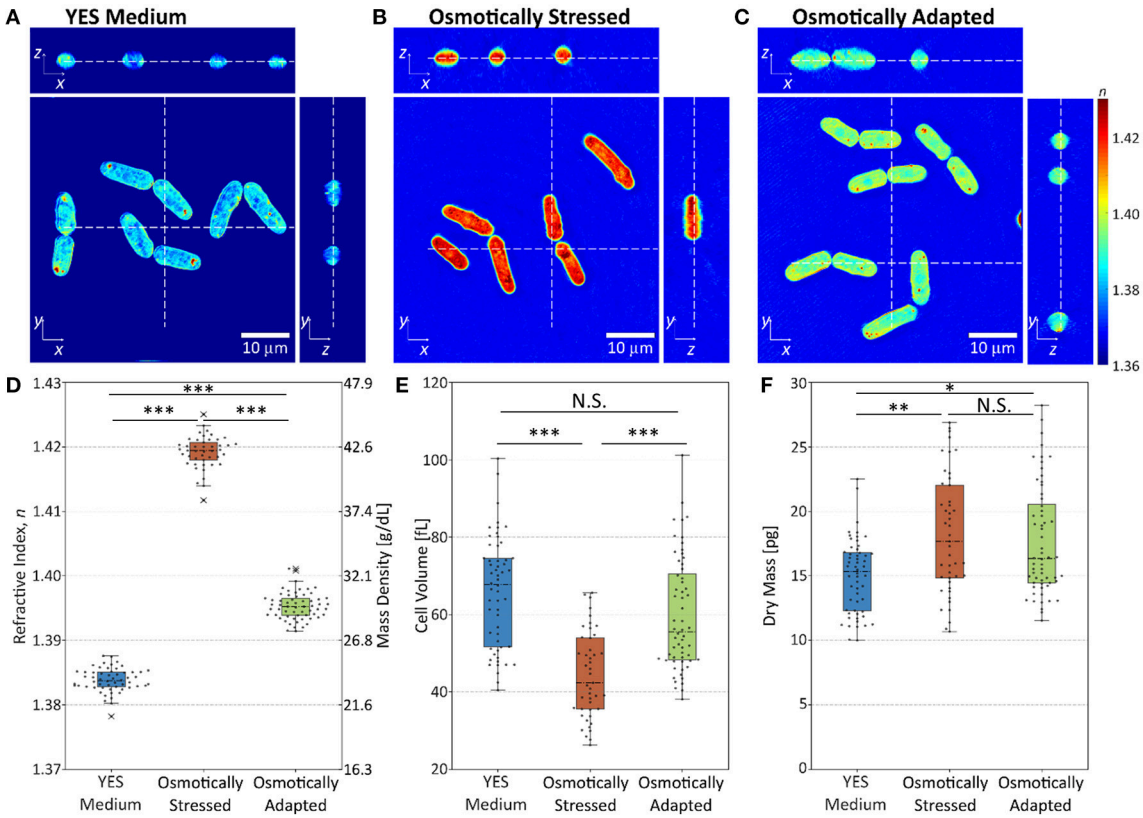

FIGURE 3 | The effect of osmotic stress and adaptation on yeast cells. **(A–C)** Cross-sectional slices in the *x-y*, *y-z*, and *x-z* planes of 3D RI tomograms of **(A)** control in YES medium, **(B)** osmotically stressed, and **(C)** osmotically adapted yeast cells. The scale bars correspond to 10 µm, and dashed lines indicate corresponding cross-sectional slices. **(D–F)** The distribution of **(D)** RI, **(E)** cell volume, and **(F)** dry mass of control, osmotically stressed, and osmotically adapted yeast cells, respectively. The box plot indicates the interquartile ranges (IQR) with a line at the median. The whiskers extend to the data within the 1.5 IQR of the respective quartile. Outliers outside of 1.5 IQR are marked as × (for each condition, $N > 45$). $^{*}p < 0.01$; $^{**}p < 0.001$; $^{***}p < 0.0001$.

with lowering intracellular pH is not sufficient for keeping the cells in a growth-arrested state.

To provide additional insight into the physical structure of the internal cellular environment, we analyzed the motion of self-aggregated viral capsid proteins (GFP − µNS, see section Materials and Methods and the **Supplementary Material**) in the cytoplasm of yeast (*S. cerevisiae*). Following the analysis of Munder et al., we considered the correlation of two subsequent particle displacements $\overrightarrow{\delta x}$ and $\overrightarrow{\delta x'}$ [14]. The projection of the second displacement onto the direction of the first one is $\equiv \overrightarrow{\delta x'} \cdot \frac{\overrightarrow{\delta x}}{|\overrightarrow{\delta x}|}$. For small displacements, we expect this quantity to be a linear function of the initial particle displacement, $c = b|\overrightarrow{\delta x}|$. For a viscous material the slope b vanishes, whereas for an elastic material $b = -1/2$. The value of b consequently serves as a proxy for the rigidity of the cytoplasm. In the previous work it was found that healthy, log phase cells displayed $b \approx -0.17$ whereas acidified cells showed $b \approx -0.34$ [14]. In **Figure 4**, the projection c defined above is shown for *S. cerevisiae* exposed to 0.8 M sorbitol (circles) and 1 M sorbitol (squares). Also shown are the scalings of c expected for log phase cells (dashed line) and acidified cells (solid line). It is clear that osmotic compression alone does not significantly alter the value of b, suggesting that the elastic properties of the cytoplasm remain unaffected by osmotic compression.

Intracellular pH Affects Mass Density Recovery Rate After Osmotic Stress

Our findings so far show that metabolic arrest induced by an acidified cytoplasm is correlated with higher intracellular mass density, while inducing the same high mass density by osmotic stress alone does not arrest cell growth. To confirm that only cells with low intracellular pH stay in the growth-arrested state and do not recover, we followed the recovery of osmotically stressed cells after changing their intracellular pH by measuring time-lapse RI tomograms. We induced osmotic stress on yeast cells by adding 1.2 M sorbitol to the phosphate buffer with 2% glucose in pH 7.5 (osmolality 2.03 ± 0.03 Osmol/kg) and pH 6.0 (osmolality 2.02 ± 0.04 Osmol/kg) as before, and then added DNP to equilibrate the intracellular pH to that of the surrounding medium. As a control, we added 1.2 M sorbitol to the YES medium. We then measured tomograms every 10 min in order to explore the

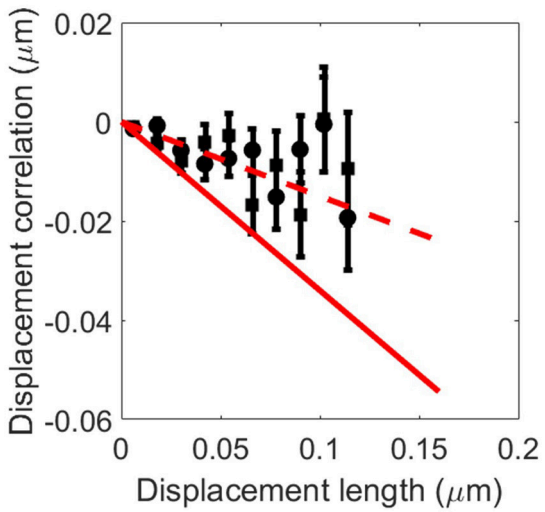

FIGURE 4 | Quantitative analysis of particle tracking. The dependence of the displacement correlation as defined in the main text, as function of the displacement length for yeast (*S. cerevisiae*) treated with 0.8 M sorbitol (circles) and 1 M sorbitol (squares). The solid line correspond to the dependence of the correlation on displacement length for acidified cells, and the dashed line corresponds to healthy, log-phase cells from Munder et al. [14]. The displacement correlation measured in osmotically stressed cells is consistent with healthy cells, but not with acidified cells.

change of mass density and volume of yeast cells after osmotic stress.

Figure 5A shows time-lapse tomograms of yeast cells with different intracellular pH when osmotic stress was induced at $t = 0$ min. The control yeast cells (first row in **Figure 5A**) recovered their RI-value promptly after the osmotic stress, exhibiting an exponential decay of mean RI-value. Meanwhile, the mean RI-values of yeast cells with an intracellular pH of 7.5 (second row in **Figure 5A**) stayed stable for the first 30 min (most probably for adapting to their transfer from YES medium into phosphate buffer medium), before the RI started to recover. More interestingly, the mean RI-values of yeast cells with the intracellular pH of 6.0 (third row in **Figure 5A**) did not change during the 60 min of observation (yellow box plots in **Figure 5B**). While only increasing intracellular mass density at neutral pH was followed by a recovery of intracellular RI and mass density, the lack of such recovery in low intracellular pH implies that physical and mechanical changes of the cytoplasm, associated with growth arrest, have occurred.

To test the mechanical status of the fission yeast cytoplasm it is possible to remove the rigid cell wall (spheroplasting) and then to follow their rounding up—or the lack thereof [14]. As shown in **Figures 6A,B**, osmotically stressed yeast cells in YES medium and with a intracellular pH of 7.5 rounded up into a spherical shape to minimize the surface to volume ratio after spheroplasting, which indicated that the cytoplasm was in a liquid-like state [35, 36]. They also had slightly lower RI-values than osmotically stressed yeast cells without spheroplasting, which might have induced an increase in volume. However, osmotically stressed yeast cells with an intracellular pH of 6.0 did not acquire a round shape upon cell wall removal and exhibited increased RI-values (**Figure 6C**), which demonstrated the transition of the cytoplasm into a solid state with an inherent elastic stiffness that prevented rounding up.

Increased Intracellular Mass Density Is Associated With but Not Sufficient For Cell Stiffening

We had previously demonstrated that the acidified cytoplasm undergoes a liquid-to-solid transition [14] and showed now that this coincides with an increase in the intracellular mass density. However, our data suggest that a sudden mass density increase of the cytoplasm may not be sufficient to promote this transition. In order to quantify and relate the mechanical changes to mass density changes in the yeast cytoplasm, we carried out AFM indentation experiments and ODT measurements of osmotically stressed and adapted yeast cells taken from identical batches. To extract and compare the mechanical properties of yeast cytoplasm using a Hertz model with AFM, it is important to apply the method to the same spherical geometry. This can be achieved by first removing the cell wall of *S. pombe* and then changing the intracellular pH. However, removal of the cell wall also requires the use of high molalities of sorbitol to prevent cell lysis.

Thus, to measure the effect of intracellular pH only, it is important to adapt the cells to these high molarities. To this end, we first measured spheroplasts of cells that had been adapted to hypertonic medium overnight before cell wall removal and adjustment of pH, as shown in **Figure 7A**. Yeast spheroplasts with low intracellular pH had a higher RI, which is directly correlated with higher mass density, than with neutral pH as shown in **Figure 7B**. Importantly, the apparent Young's modulus of the acidified spheroplasts was significantly higher ($E = 17.6 \pm 0.2$ kPa; mean ± SEM) compared to the Young's modulus of spheroplasts with a neutral intracellular pH ($E = 4.3 \pm 0.1$ kPa) (**Figure 7C**). These results demonstrate that acidification of the yeast cytoplasm coincides with mass density increase and an overall stiffness increase.

To determine if an increased intracellular mass density is sufficient to stiffen the yeast, we osmotically stressed cells cultured in YES medium by addition of 1.2 M sorbitol, then immediately removed the cell wall, and subjected the spheroplasts to ODT and AFM indentation measurements (**Figure 7D**). In agreement with the notion that sorbitol induces osmotic stress, the RI-values of cells with a neutral intracellular pH already exhibited a high RI. Interestingly, the intracellular mass density of yeast spheroplasts with a low intracellular pH was not further increased (**Figure 7E**). Importantly, the apparent Young's modulus of the acidified spheroplasts was significantly higher ($E = 13.1 \pm 0.2$ kPa; mean ± SEM) compared to the Young's modulus determined for spheroplasts with a neutral intracellular pH ($E = 6.3 \pm 0.1$ kPa), despite the similar mass density (**Figure 7F**). These results unambiguously demonstrate that increased intracellular mass density does not by itself lead to cell stiffening. Apparently, the cytoplasm requires, in addition to increased content crowding, other mechanisms to acquire its mechanical stability and to arrest growth.

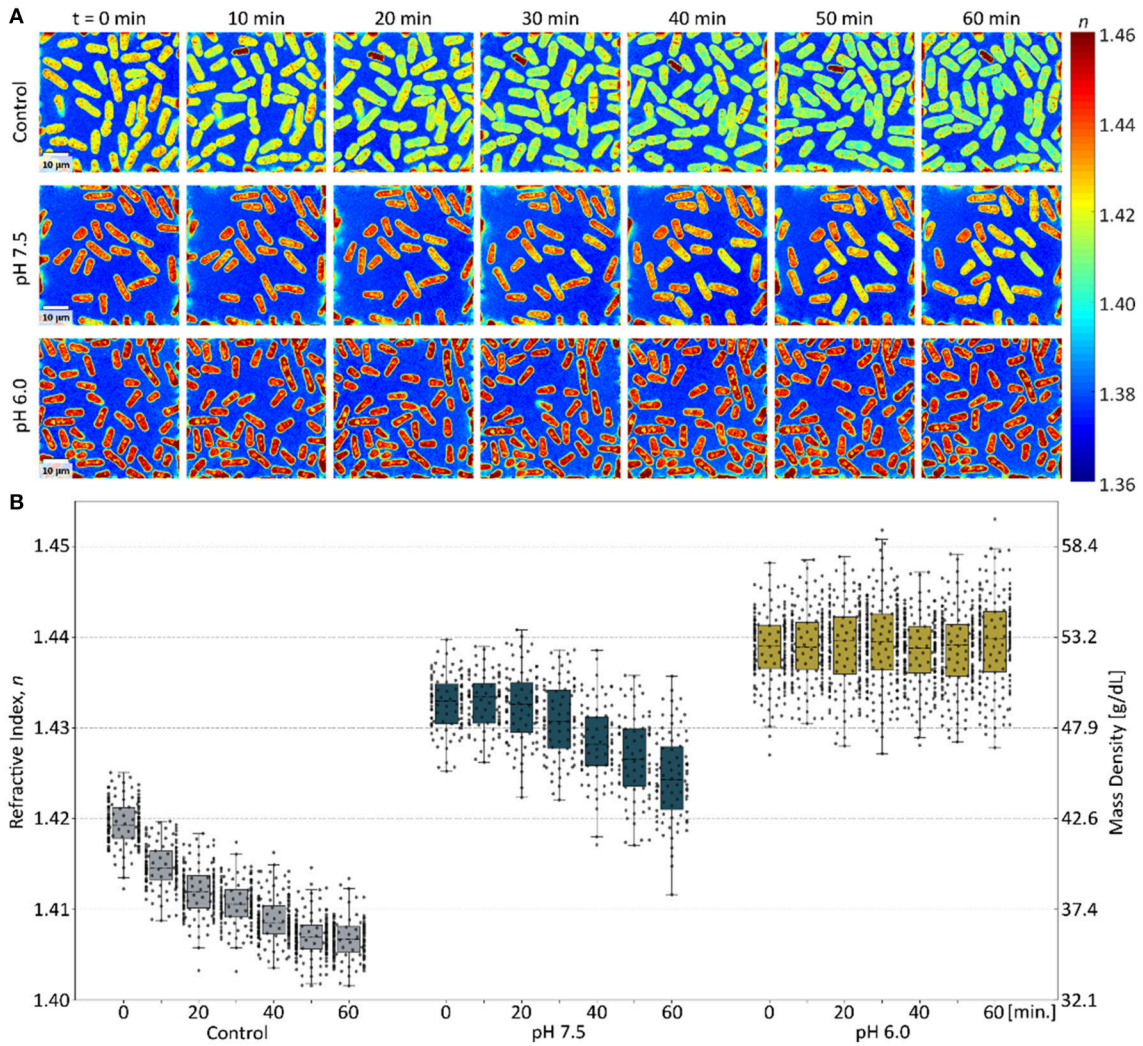

FIGURE 5 | The effect of intracellular pH on the recovery rate of the mass density of yeast cells after osmotic stress. **(A)** The cross-sectional slices of time-lapse 3D RI tomograms of yeast cells with different intracellular pH, acquired every 10 min after osmotic stress. The scale bar indicates 10 µm. **(B)** The mean refractive index distribution of osmotically stressed cells in YES medium (gray, $N > 120$), at pH 7.5 (blue, $N > 70$) and at pH 6.0 (yellow, $N > 150$). The box plot indicates the interquartile ranges (IQR) with a line at the median. The whiskers extend to the data within the 1.5 IQR of the respective quartile. Outliers outside of 1.5 IQR are marked as ×.

DISCUSSION

In this study, we investigated the relationship between intracellular mass density, changes in intracellular pH and stiffness of growing and arrested *S. pombe* yeast cells. We adopted the method of Munder et al. for lowering intracellular pH in yeast cells [14]. We employed ODT to measure the RI-values and evaluate the mass density of yeast cells, and found that mass density is increased in the acidified yeast cytoplasm. We then showed that increasing mass density triggered by osmotic stress is not sufficient to promote a permanent transition into a mechanically stiff and growth-arrested state. We confirmed that yeast cells with acidified cytoplasm exhibited characteristics of dormancy as they did not exhibit any distinct mass density change after osmotic stress and showed no rounding up upon cell wall removal. We assessed the mechanical properties of acidified and neutral yeast cytoplasm using AFM. We demonstrated that an increase in stiffness is accompanied with an increase in the intracellular mass density. However, increasing mass density of active yeast cells by osmotic stress was not associated with an increase in stiffness.

In this work, we have, for the first time, employed ODT to evaluate mass density changes and total dry mass of the yeast cytoplasm. We provided evidence for the mechanism of yeast cells to lose water and increase mass density when dormancy is induced by lowering intracellular pH. This crowded intracellular content leads definitely to a change in the physical properties of the cytoplasm that were so far explored using traditional techniques such as exogeneous particle tracking [14, 37, 38]. Various explanations have previously been proposed for the

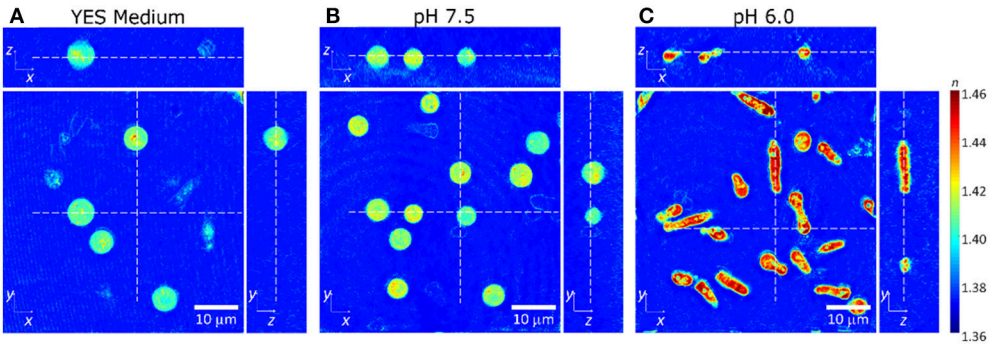

FIGURE 6 | The cross-sectional slices of refractive index tomograms of yeast in **(A)** YES medium with 1.2 M sorbitol, **(B)** phosphate buffer in pH of 7.5 and **(C)** pH 6.0 with 1.2 M sorbitol and DNP, after the removal of cell wall. The scale bar indicates 10 µm.

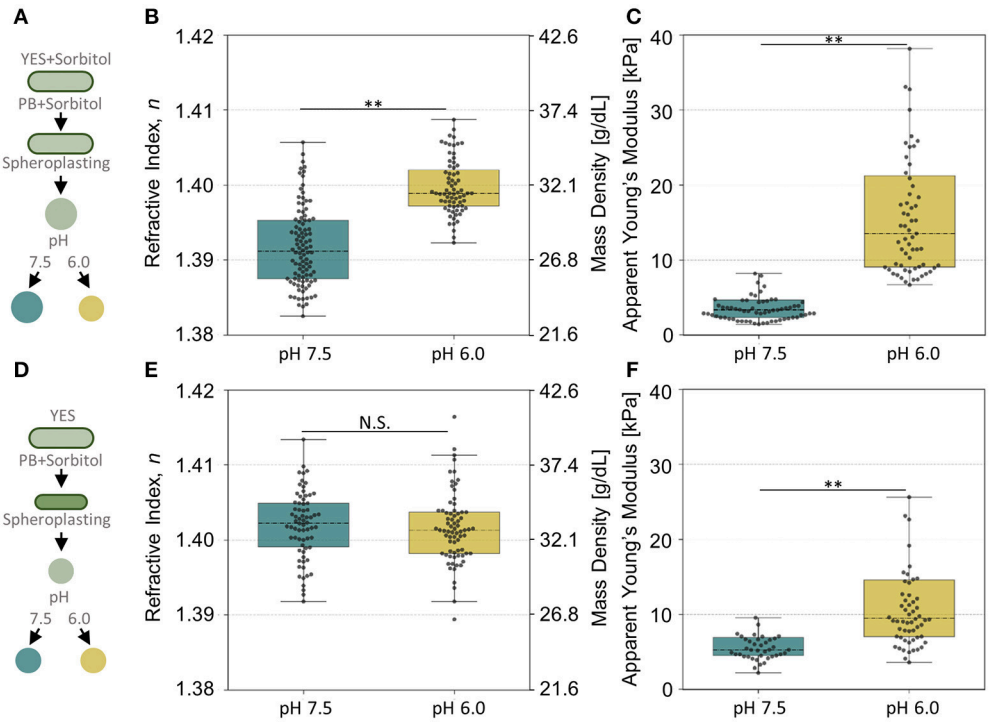

FIGURE 7 | Stiffness and mass density of yeast cells with different intracellular pH during or after adaptation to osmotic stress. **(A,D)** Schematic diagram for cell culture, spheroplasting in phosphate buffer (PB) with sorbitol and pH adjustment for **(A)** overnight osmotically adapted and **(D)** osmotically stressed *S. pombe*. **(B,E)** The distribution of mean refractive index of yeast cells with intracellular pH of 7.5 and 6.0 in **(B)** osmotic adaptation ($N > 70$) and **(E)** osmotic stress ($N > 70$). **(C,F)** The distribution of the apparent Young's modulus of spheroplasts in the intracellular pH of 7.5 and 6.0 in **(C)** osmotic adaptation ($N > 60$) and **(F)** osmotic stress ($N > 40$). The box plot indicates the interquartile ranges (IQR) with a line at the median. The whiskers extend to the data within the 1.5 IQR of the respective quartile. Outliers outside of 1.5 IQR are not shown. $^{**}p < 0.001$.

nature of these changes. Some suggested that the cytoplasm undergoes a glass transition due to increased mass density [39]. Others described a cytoplasm as water-containing matrix formed by a cytoskeletal network that is behaving as a hydrogel [40]. We here demonstrate that increasing the mass density of cells will not by itself result in stiffening and growth arrest of yeast cells. We show that the cytoplasm of metabolically arrested cells acquires, along with an increased mass density, solid-like characteristics. We have also explored that different degrees of compression increased the crowding of the cytoplasm using particle tracking method (**Supplementary Figures 3, 4**). In addition, similar to Munder et al. we have analyzed the isoelectric points of all proteins in the *S. pombe* yeast proteome. We found, in agreement with other studies [41], that the isoelectric points of the proteins are clustered in two distinct peaks one in the acidic and the other in the basic pH range (**Supplementary Figure 2**). When the pH

drops to the isoelectric points, the proteins fall out of solution and form macromolecular aggregates. One plausible outcome of the macromolecular aggregation is a reduction in the internal osmotic pressure of the cell and thus water loss and densification of the cytosol. We thus suggest that the combination of high mass density and reinforcing the cytoplasm with some percolated network of macromolecular assemblies is necessary for providing the cells with the mechanical stability needed for enduring harsh environmental conditions and ultimately survival.

Still, in order to profoundly unravel the structure and the organization of the solid cytoplasmic network, it is necessary to explore the response of these physical properties at various time scales. This could be achieved with the use of AFM dynamic probing of the mechanical properties at different frequencies. Using AFM provides a straight-forward measurement of cytoplasm, nevertheless, it requires steps of removing the yeast cell wall, which could potentially alter cell properties, and current analysis assumes homogeneity of the sample. Thus, there is a growing interest in using non-invasive optical methods to probe mechanical properties of soft materials such as Brillouin microscopy [42, 43] and the temporal correlations of time-lapse quantitative phase microscopy [44, 45].

Taken together, we present here a study that augments the field of phase transitions in dormant organisms with an insight into the optical and mechanical properties of the cytoplasm. We defined the interplay between intracellular mass density, stiffness and dormancy. Further studies for exploring the key factors and the organization of the solid cytoplasm will be essential to understand the underlying mechanisms of these organisms to initiate dormancy.

AUTHOR CONTRIBUTIONS

SAb, KK, TF, AE, RS, SM, H-SK, SAl, VZ, and JG contributed to the conception and design of the study; SAb prepared the cells, conducted the AFM measurements, analyzed, and interpreted AFM data; KK prepared the cells, conducted the ODT measurements, analyzed, and interpreted ODT data; TF, AE provided the cells and the mediums, provided biological support for experiments; DM performed particle tracking, DM and VZ interpreted particle tracking data; RS and SM contributed to experiment performance; H-SK and VZ contributed to the theoretical aspect of data interpretation; SAb and KK wrote the first draft of the manuscript; TF, DM, VZ, and JG contributed to manuscript revision.

FUNDING

The authors acknowledge financial support from the Volkswagen Foundation (research grant 92847 to KK, HK, AE, VZ, SAl, and JG), the European Union's Horizon 2020 research and innovation programme under the Marie Sklodowska-Curie (grant agreement No 641639 to SAb and JG), the Max Planck Gesellschaft core funding (TF, AE, VZ, SAl), the German Federal Ministry of Research and Education (BMBF 031A359A to TF), and the Alexander von Humboldt Stiftung (Alexander von Humboldt Professorship to JG).

ACKNOWLEDGMENTS

We thank the Microstructure Facility at the Center for Molecular and Cellular Bioengineering (CMCB) at Technische Universität Dresden and JPK Instruments AG in Berlin for excellent support. We are also grateful to Gheorghe Cojoc, Joan-Carles Escolano, Paul Müller, Anna Taubenberger, Elke Ulbricht, Torsten Müller, Vamshidhar Gade, Teymuras Kurzchalia, Elisabeth Fischer-Friedrich, and Kamran Hosseini for helpful discussions and technical support.

SUPPLEMENTARY MATERIAL

The Supplementary Material for this article can be found online at: https://www.frontiersin.org/articles/10.3389/fphy.2018.00131/full#supplementary-material

REFERENCES

1. Hyman AA, Weber CA, Jülicher F. Liquid-liquid phase separation in biology. *Annu Rev Cell Dev Biol.* (2014) **30**:39–58. doi: 10.1146/annurev-cellbio-100913-013325
2. Alberti S. Phase separation in biology. *Curr Biol.* (2017) **27**:R1097–102. doi: 10.1016/j.cub.2017.08.069
3. Banani SF, Lee HO, Hyman AA, Rosen MK. Biomolecular condensates: organizers of cellular biochemistry. *Nat Rev Mol Cell Biol.* (2017) **18**:285–98. doi: 10.1038/nrm.2017.7
4. Brangwynne CP, Eckmann CR, Courson DS, Rybarska A, Hoege C, et al. Germline P granules are liquid droplets that localize by controlled dissolution/condensation. *Science* (2009) **324**:1729–32. doi: 10.1126/science.1172046
5. Patel A, Lee HO, Jawerth L, Maharana S, Jahnel M, Hein MY, et al. A liquid-to-solid phase transition of the ALS protein FUS accelerated by disease mutation. *Cell* (2015) **162**:1066–77. doi: 10.1016/j.cell.2015.07.047
6. van Zanten M, Koini MA, Geyer R, Liu Y, Brambilla V, Bartels D, et al. Seed maturation in *Arabidopsis thaliana* is characterized by nuclear size reduction and increased chromatin condensation. *Proc Natl Acad Sci USA.* (2011) **108**:20219–24. doi: 10.1073/pnas.1117726108
7. van Vliet S. Bacterial dormancy: how to decide when to wake up. *Curr Biol.* (2015) **25**:R753–5. doi: 10.1016/j.cub.2015.07.039
8. Erkut C, Kurzchalia TV. The *C. elegans* dauer larva as a paradigm to study metabolic suppression and desiccation tolerance. *Planta* (2015) **242**:389–96. doi: 10.1007/s00425-015-2300-x
9. Orij R, Urbanus ML, Vizeacoumar FJ, Giaever G, Boone C, Nislow C, et al. Genome-wide analysis of intracellular pH reveals quantitative control of cell division rate by pHc in *Saccharomyces cerevisiae*. *Genome Biol.* (2012) **13**:R80. doi: 10.1186/gb-2012-13-9-r80
10. Dechant R, Binda M, Lee SS, Pelet S, Winderickx J, Peter M. Cytosolic pH is a second messenger for glucose and regulates the PKA pathway through V-ATPase. *EMBO J.* (2010) **29**:2515–26. doi: 10.1038/emboj.2010.138
11. Canetta E, Walker GM, Adya AK. Nanoscopic morphological changes in yeast cell surfaces caused by oxidative stress: an atomic force microscopic study. *J Microbiol Biotechnol.* (2009) **19**:547–55. doi: 10.4014/jmb.0809.515
12. Adya AK, Canetta E, Walker GM. Atomic force microscopic study of the influence of physical stresses on *Saccharomyces cerevisiae*

and *Schizosaccharomyces pombe*. *FEMS Yeast Res.* (2006) **6**:120–8. doi: 10.1111/j.1567-1364.2005.00003.x
13. Delarue M, Hartung J, Schreck C, Gniewek P, Hu L, Herminghaus S, et al. Self-driven jamming in growing microbial populations. *Nat Phys.* (2016) **12**:762–6. doi: 10.1038/nphys3741
14. Munder MC, Midtvedt D, Franzmann T, Nüske E, Otto O, Herbig M, et al. A pH-driven transition of the cytoplasm from a fluid- to a solid-like state promotes entry into dormancy. *Elife* (2016) **5**:1–30. doi: 10.7554/eLife.09347
15. Takeda M, Ina H, Kobayashi S. Fourier-transform method of fringe-pattern analysis for computer-based topography and interferometry. *J Opt Soc Am A* (1982) **72**:156–160. doi: 10.1364/JOSA.72.000156
16. Cuche E, Marquet P, Depeursinge C. Spatial filtering for zero-order and twin-image elimination in digital off-axis holography. *Appl Opt.* (2000) **39**:4070–5. doi: 10.1364/AO.39.004070
17. Wolf E. Three-dimensional structure determination of semi-transparent objects from holographic data. *Opt Commun.* (1969) **1**:153–6. doi: 10.1016/0030-4018(69)90052-2
18. Sung Y, Choi W, Fang-Yen C, Badizadegan K, Dasari RR, Feld MS. Optical diffraction tomography for high resolution live cell imaging. *Opt Express* (2009) **17**:266–277. doi: 10.1364/OE.17.000266
19. Kim K, Yoon H, Diez-Silva M, Dao M, Dasari RR, Park Y. High-resolution three-dimensional imaging of red blood cells parasitized by Plasmodium falciparum and *in situ* hemozoin crystals using optical diffraction tomography. *J Biomed Opt.* (2014) **19**:011005. doi: 10.1117/1.JBO.19.1.011005
20. Müller P, Schürmann M, Guck J. The theory of diffraction tomography. *arXiv:1507.00466* (2015).
21. Zhao H, Brown PH, Schuck P. On the distribution of protein refractive index increments. *Biophys J.* (2011) **100**:2309–17. doi: 10.1016/j.bpj.2011.03.004
22. Gautier HOB, Thompson AJ, Achouri S, Koser DE, Holtzmann K, Moeendarbary E, et al. Atomic force microscopy-based force measurements on animal cells and tissues. *Methods Cell Biol.* (2015) **125**:211–35. doi: 10.1016/bs.mcb.2014.10.005
23. Radmacher M. Studying the mechanics of cellular processes by atomic force microscopy. *Methods Cell Biol.* (2007) **83**:347–72. doi: 10.1016/S0091-679X(07)83015-9
24. Hertz H. Über die berührung fester elastischer körper. *J Reine Angew Math.* (1881) **92**:156–71.
25. Yango A, Schäpe J, Rianna C, Doschke H, Radmacher M, Rotsch C, et al. Measuring the viscoelastic creep of soft samples by step response AFM. *Soft Matter* (2016) **12**:8297–306. doi: 10.1039/C6SM00801A
26. Dokukin ME, Guz N V, Sokolov I. Quantitative study of the elastic modulus of loosely attached cells in AFM indentation experiments. *Biophys J.* (2013) **104**:2123–31. doi: 10.1016/j.bpj.2013.04.019
27. Glaubitz M, Medvedev N, Pussak D, Hartmann L, Schmidt S, Helm CA, et al. A novel contact model for AFM indentation experiments on soft spherical cell-like particles. *Soft Matter* (2014) **10**:6732–41. doi: 10.1039/C4SM00788C
28. Sbalzarini IF, Koumoutsakos P. Feature point tracking and trajectory analysis for video imaging in cell biology. *J Struct Biol.* (2005) **151**:182–95. doi: 10.1016/j.jsb.2005.06.002
29. De Virgilio C. The essence of yeast quiescence. *FEMS Microbiol Rev.* (2012) **36**:306–39. doi: 10.1111/j.1574-6976.2011.00287.x
30. Gray JV, Petsko GA, Johnston GC, Ringe D, Singer RA, Werner-Washburne M. "Sleeping Beauty": quiescence in *Saccharomyces cerevisiae*. *Microbiol Mol Biol Rev.* (2004) **68**:187–206. doi: 10.1128/MMBR.68.2.187-206.2004
31. Neiman AM. Sporulation in the budding yeast *Saccharomyces cerevisiae*. *Genetics* (2011) **189**:737–65. doi: 10.1534/genetics.111.127126
32. Valcourt JR, Lemons JMS, Haley EM, Kojima M, Demuren OO, Coller HA. Staying alive. *Cell Cycle* (2012) **11**:1680–96. doi: 10.4161/cc.19879
33. Erkut C, Gade VR, Laxman S, Kurzchalia TV. The glyoxylate shunt is essential for desiccation tolerance in *C. elegans* and budding yeast. *Elife* (2016) **5**:1–24. doi: 10.7554/eLife.13614
34. Shen B, Hohmann S, Jensen RG, Bohnert AH. Roles of sugar alcohols in osmotic stress adaptation. Replacement of glycerol by mannitol and sorbitol in yeast. *Plant Physiol.* (1999) **121**:45–52.
35. Kelly FD, Nurse P. *De novo* growth zone formation from fission yeast spheroplasts. *PLoS ONE* (2011) **6**:e27977. doi: 10.1371/journal.pone.0027977
36. Sipiczki M, Heyer W-D, Kohli J. Preparation and regeneration of protoplasts and spheroplasts for fusion and transformation of *Schizosaccharomyces pombe*. *Curr Microbiol.* (1985) **12**:169–73. doi: 10.1007/BF01567671
37. Dix JA, Verkman AS. Crowding effects on diffusion in solutions and cells. *Annu Rev Biophys.* (2008) **37**:247–63. doi: 10.1146/annurev.biophys.37.032807.125824
38. Tolić-Nørrelykke IM, Munteanu E-L, Thon G, Oddershede L, Berg-Sørensen K. Anomalous diffusion in living yeast cells. *Phys Rev Lett.* (2004) **93**:078102. doi: 10.1103/PhysRevLett.93.078102
39. Parry BR, Surovtsev IV, Cabeen MT, O'Hern CS, Dufresne ER, Jacobs-Wagner C. The bacterial cytoplasm has glass-like properties and is fluidized by metabolic activity. *Cell* (2014) **156**:183–94. doi: 10.1016/j.cell.2013.11.028
40. Fels J, Orlov SN, Grygorczyk R. The hydrogel nature of mammalian cytoplasm contributes to osmosensing and extracellular pH sensing. *Biophys J.* (2009) **96**:4276–85. doi: 10.1016/j.bpj.2009.02.038
41. Kozlowski LP. Proteome-pI: proteome isoelectric point database. *Nucleic Acids Res.* (2017) **45**:D1112–6. doi: 10.1093/nar/gkw978
42. Schlüßler R, Möllmert S, Abuhattum S, Cojoc G, Müller P, Kim K, et al. Mechanical mapping of spinal cord growth and repair in living Zebrafish Larvae by Brillouin imaging. *Biophys J.* (2018) **115**:911–23. doi: 10.1016/j.bpj.2018.07.027
43. Scarcelli G, Yun SH. Confocal Brillouin microscopy for three-dimensional mechanical imaging. *Nat Photonics* (2008) **2**:39–43. doi: 10.1038/nphoton.2007.250
44. Cerbino R, Trappe V. Differential dynamic microscopy: probing wave vector dependent dynamics with a microscope. *Phys Rev Lett.* (2008) **100**:188102. doi: 10.1103/PhysRevLett.100.188102
45. Wang R, Wang Z, Millet L, Gillette MU, Levine AJ, Popescu G. Dispersion-relation phase spectroscopy of intracellular transport. *Opt Express* (2011) **19**:20571–9. doi: 10.1364/OE.19.020571

Conflict of Interest Statement: SAb is employed by JPK Instruments AG, Berlin.

The remaining authors declare that the research was conducted in the absence of any commercial or financial relationships that could be constructed as a potential conflict of interest.

Copyright © 2018 Abuhattum, Kim, Franzmann, Eßlinger, Midtvedt, Schlüßler, Möllmert, Kuan, Alberti, Zaburdaev and Guck. This is an open-access article distributed under the terms of the Creative Commons Attribution License (CC BY). The use, distribution or reproduction in other forums is permitted, provided the original author(s) and the copyright owner(s) are credited and that the original publication in this journal is cited, in accordance with accepted academic practice. No use, distribution or reproduction is permitted which does not comply with these terms.